Mater. Res. Soc. Symp. Proc. Vol. 1148 © 2009 Materials Research Society 1148-PP10-01

Porosity through reduction in metal oxides

Daniel P. Shoemaker, Serena A. Corr and Ram Seshadri
Materials Research Laboratory, University of California,
Santa Barbara, CA 93106, U.S.A.

ABSTRACT

Routes to porous materials with nanoscale dimensions have been investigated. In the first example presented, porous manganese oxide has been prepared by leaching Ni metal from a nickel-manganese oxide precursor *via* reduction. Electron microscopy studies have revealed the presence of Ni nanoparticles on the surface, and also embedded within the porous MnO matrix. Magnetic measurements have shown exchange bias between the ferromagnetic Ni nanoparticles and the antiferromagnetic MnO phase. In the second system studied, porous nanostructures of rutile VO_2 and corundum V_2O_3 have been prepared by reduction of amine-templated $V_2O_{5-\delta}$ nanoscrolls. The porosity of these materials has been probed by electron microscopy, N_2 sorption measurements and thermogravimetric analysis.

INTRODUCTION

Porous materials have received considerable attention in recent years owing to their potential applications in a number of areas. In particular, their high surface areas make them attractive candidates in catalysis, sensors, batteries and fuel cell technology.[1-3] A typical route to porous materials is to employ a sacrificial component in the structure which may be leached during a subsequent heat treatment. For example, hierarchically porous materials may be formed when oxides containing Zn are reduced at high temperatures. The resulting metallic Zn can be removed leading to a porous structure. Hierarchically porous manganese oxide [4, 5] and rutile titania [6] have been prepared in this manner. This type of porous material is of particular interest since the larger pores allow for greater flow rates through the material, while the smaller pores maintain the high surface area. Regenerative porosity has been found to occur in hierarchically porous MnO prepared by reducing sintered macroporous Mn_2O_4 pellets to induce mesopore formation.[7]

Our focus lies in the preparation and characterization of functional porous materials. Here we present two porous systems: the first a nickel-manganese oxide with magnetic functionality associated with exchange bias and the second, a family of porous vanadium oxide nanostructures whose electrical transport properties have previously been probed. Equipped with the knowledge that cation reduction will drive transformations by leaching O and creating free volume for diffusion, we have investigated phases which exhibit magnetic functionality and can be oxidized or reduced in moderate temperatures. Magnetic exchange bias can be observed when the composite is a majority antiferromagnetic (AFM) phase with small ferromagnetic (FM) particles or planes embedded within. Exchange bias is produced by field-cooling the composite below the ordering temperature of the AFM and can shift and broaden magnetic hysteresis loops. The crucial requirement in an exchange biased architecture is a high proportion of FM spins that are on the FM/AFM interface. For a thorough review of exchange biased nanostructures, see the article by Nogués, *et al*.[8] Hydrogen reduction of ternary transition metal oxides is a facile route to granular exchange-biased FM/AFM composites. Porosity can be induced by reduction of

either (or both) cation species. Some key advantages of this process are monodisperse nanoparticles, sharp interfaces between the two phases, a self-limiting precipitation reaction, preservation of overall sample shape and size, and scalability.

Reduction routes have also been employed to prepare nanotubes of rutile VO_2 or corundum V_2O_3 from amine-templated $V_2O_{5-\delta}$ nanoscrolls. Electron microscopy studies of these nanotubes have shown that these products are porous and N_2 sorption studies reveal pores in the size range of 2-50 nm. Here we present Barrett-Joyner-Halenda (BJH) analysis of the N_2 sorption data for a range of samples. We also show that the amine molecules used to prepare the parent $V_2O_{5-\delta}$ nanoscrolls acts as sacrificial pore formers by studying the thermogravimetric analysis of a series of nanotube products.

EXPERIMENT

Nickel-manganese oxide

The precursor is a tetragonal spinel $Ni_xMn_{3-x}O_4$ with x between 0.15 and 0.6. Metal oxalates are coprecipitated from acetates and calcined in air at 1000ºC-1200ºC for 18h, then water quenched to maintain phase purity.[9] A single phase precursor is preferred to ensure a uniform distribution of Ni precipitates in the finished composite. The spinel is reduced in flowing 5% H_2/N_2 gas in a tube furnace at 725ºC for 2h and slow-cooled.

Porous vanadium oxides

$V_2O_{5-\delta}$ nanoscrolls were prepared according to previous reports.[10] Briefly, vanadium (V) oxide (1.81 g, 0.01 mol) dispersed in 15 mL deionized water was added dropwise to a suspension of dodecylamine (1.88 g, 0.01 mol) in 15 mL ethanol. After stirring for 3 days, the resulting mixture was hydrothermally treated at 180 ^oC for 2 days. The resulting nanoscrolls were washed, dried and reduced according to Table 1. The products were characterized by transmission electron microscopy (TEM), scanning electron microscopy (SEM), N_2 sorption measurements and thermogravimetric analysis (TGA).

Table 1: 3×3 matrix showing the condition under which the reduction experiments were carried out in 5% H_2:95% N_2

A, 400°C, 1 h	B, 400°C, 3 h	C, 400°C, 6 h
D, 500°C, 1 h	E, 500°C, 3 h	F, 500°C, 6 h
G, 600°C, 1 h	H, 600°C, 3 h	J, 600°C, 6 h

DISCUSSION

Nickel-manganese oxide

Thermogravimetric analysis confirms the single-phase spinel reduces to an intermediate rocksalt (Ni,Mn)O solid solution at 400ºC, then reduction to metallic Ni begins at 550ºC. Since rocksalt MnO shares an anion sublattice with the precursor $(Ni,Mn)_3O_4$ spinel, gentle diffusion of atoms during reduction does not induce reorganization of the structure. It is imperative to

determine the extent of phase separation in Ni–MnO nanocomposites. If reduction of Ni^{2+} to *fcc* Ni is not complete, the precipitates could have a diffuse shell of (Ni,Mn)O. A sharp interface is desired not only for our investigation of exchange bias, but for the vast majority of applications of supported nanoparticle composites. Verification of the reaction producing Ni in MnO is confirmed by x-ray diffraction Rietveld refinement and thermogravimetric analysis, but an excellent gauge of the purity of the final composite is the linear convergence of the MnO lattice parameter and the Ni magnetic saturation toward their expected values. Both can be measured to great accuracy and unambiguously reveal complete reduction of Ni.[11]

Water quenching the precursor spinel leads to cracking between the grains, which are around 20 μm in extent. This grain size is maintained in the reduced composite seen in Figure 1(a).

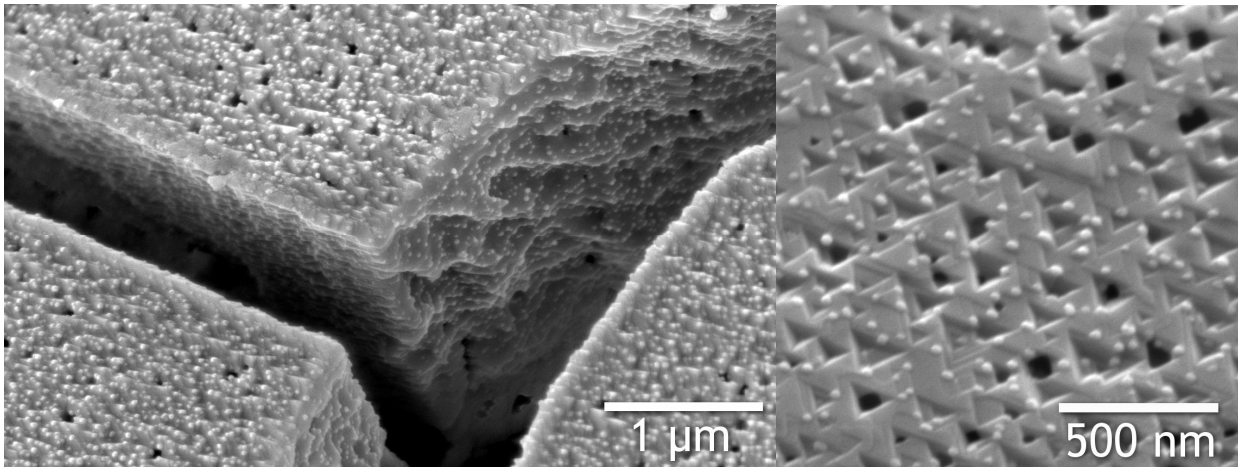

Figure 1. Scanning electron micrographs of a reduced Ni / MnO composite. In (a), the large-grained microstructure from the spinel precursor is maintained, but nanosized pores are evident and Ni nanoparticles are visible as the light dots. In (b), the as-reduced surface has triangular facets and pores, and Ni nanoparticles are about 20-50 nm in diameter.

The light spots are Ni nanoparticles on the surface of the grain. The Ni nanoparticle diameter is seen in Figure 1(b) to be about 30 nm on the surface, and is reasonably constant for all initial Ni concentrations. This particular surface has triangular MnO facets and pores, but square pores are also common, as evidenced in the conventional transmission electron micrograph in Figure 2(a). A strong relation has been observed between Ni particle size (on the MnO surface) and the specific crystallographic face of MnO upon which it lies, but focused ion beam milling has indicated that 80% of the Ni particles are *embedded within* the MnO matrix, and not on the surface or in a pore. The selected area electron diffraction pattern in Figure 2(b) shows the MnO matrix is a single crystal despite its porosity, and only a fraction of the Ni is crystallographically aligned with the matrix. Many $\{200\}_{Ni}$ diffraction spots can be seen at various orientations, and only two are labeled here.

Magnetic studies of the composites reveal the presence of significant loop shifting and broadening as a result of exchange bias. At 5 K, the hysteresis loop is broadened significantly, and field-cooling (H = 50 kOe) results in a loop that is displaced along the $-H$ direction. The

most convincing evidence for exchange bias lies in the dependence of field-cooled loop shift H_E as a function of temperature. Both the coercivity and exchange field data reveal a sharp increase upon cooling below the MnO Néel temperature of 119 K, and H_E is zero above T_N or after cooling in zero field. For a detailed investigation of magnetism and its dependence on temperature and Ni content, see reference [11].

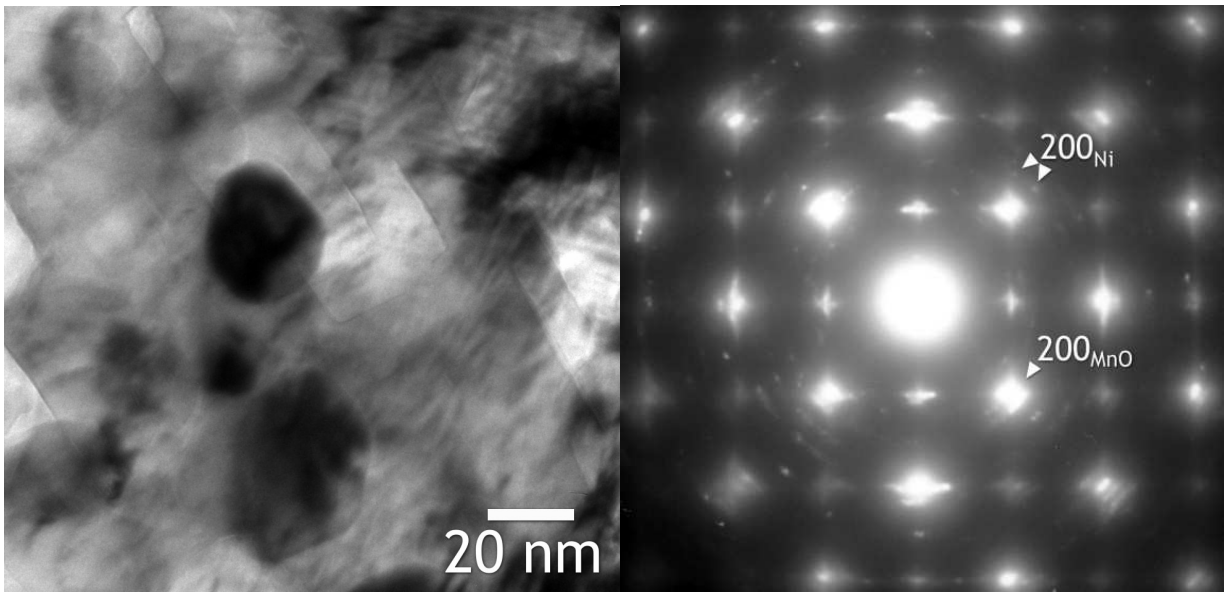

Figure 2. Conventional transmission electron microscopy (a) reveals square pores about 40 nm across in an MnO grain. The dark spots are Ni nanoparticles. In (b), the selected area diffraction of a micron-sized MnO grain confirms that the monolith is a single crystal despite its large pore volume. Many *fcc* Ni diffraction spots are visible, and only some are aligned crystallographically with the host MnO lattice.

Porous vanadium oxides

Amine-templated nanoscrolls were prepared using hydrothermal methods. Systematic reduction of these nanoscrolls allows for the preparation of porous rutile VO_2 and corundum V_2O_3 nanostructures.[10] We have found that the reduction conditions may be tuned to yield the desired phase. X-ray diffraction patterns have shown that lower reduction times and temperatures (table 1, samples A-D) produce rutile VO_2, while higher temperatures (table 1, samples F-J) yield corundum V_2O_3. Intermediate reduction conditions (table 1, sample E) give a mixture of both phases. SEM images of the post-reduced samples show a distinct change in size, shape and surface morphology when compared to the original crystalline nanoscrolls. Heating in a reducing atmosphere at progressively elevated temperatures leads to a breaking down of the nanoscrolls into shorter nanotubes, with surface roughness noted in the SEM images. Figure 3 shows SEM images of samples reduced at 500°C with increasing reduction times. The fact that these are now nanotubes as opposed to nanoscrolls is clearly evident from the images, along with the observation of porous tube walls.

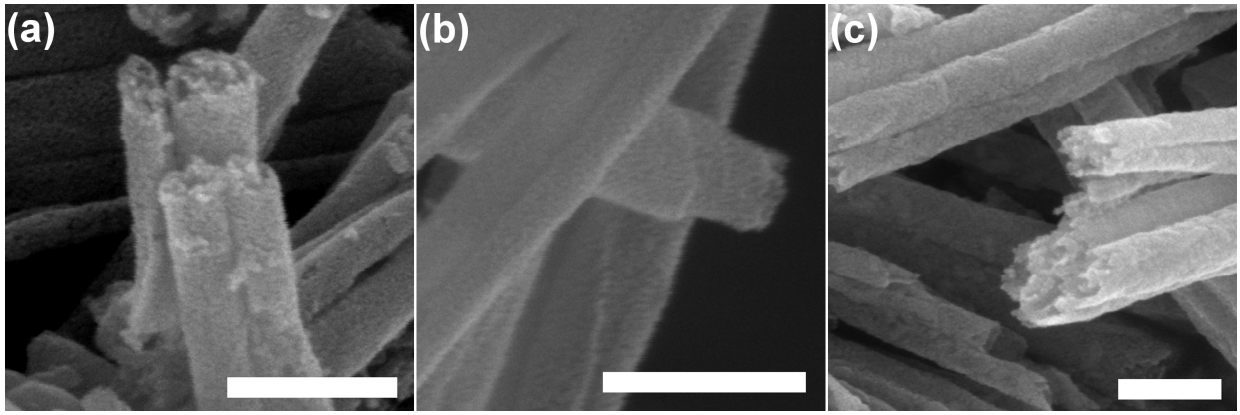

Figure 3. SEM images of $V_2O_{5-\delta}$ nanoscrolls reduced at 500°C for (a) 1 h, (b) 3 h and (c) 6 h. The scale bar in each image is 200 nm.

TEM images agree with these observations, with nanocrystalline materials noted on the surface of the reduced products (figure 4). We have previously reported the X-ray data for these samples which show that for the case of sample E (500°C, 1h) these are nanocrystals of rutile VO_2, while in the case of sample F (500°C, 6 h) they are corundum V_2O_3. In the intermediate case, a decrease in X-ray diffraction intensity is due to a lack of crystalline material in the walls of the products (figure 4b).

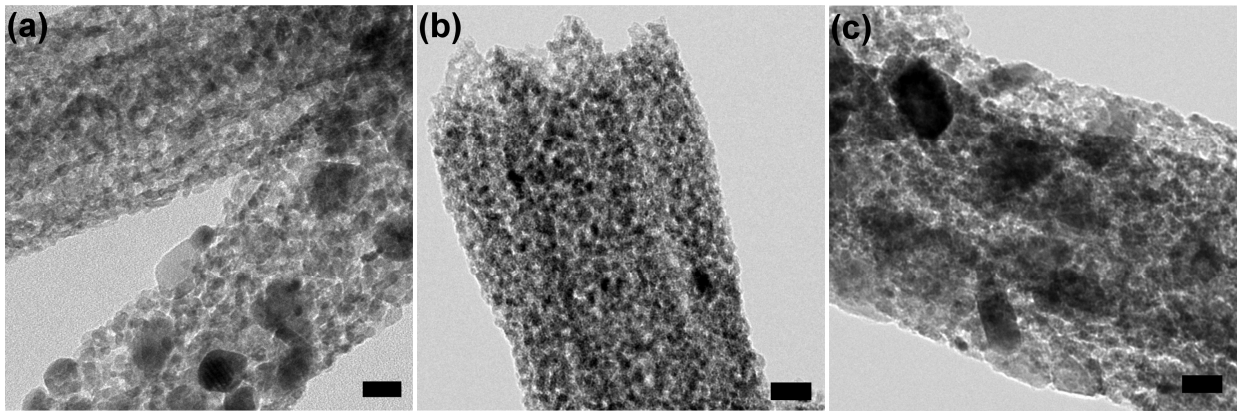

Figure 4. TEM images of $V_2O_{5-\delta}$ nanoscrolls reduced at 500°C for (a) 1 h, (b) 3 h and (c) 6 h. The porosity of the samples is evident from the images, along with the presence of nanocrystalline material. The scale bar in each image corresponds to 20 nm.

The average pore diameter has been calculated from Barrett-Joyner-Halenda (BJH) analysis of N_2 sorption isotherms. Figure 5 shows the results obtained for the samples reduced for 6 h at 400°C (sample C), 500°C (sample F) and 600°C (sample J). On increasing the reduction temperature, there is a noted decrease in the average pore diameter (66 nm, 39 nm and 15 nm on heating from 400°C to 500°C to 600°C, respectively). The specific surface area is

found to increase on going from 400°C (31 m^2/g) to 500°C (77 m^2/g), due to an increase in pore formation at higher temperatures. However, on going to 600°C, the surface area decreases to 66 m^2/g. This is most likely due to the formation of large crystallites of V_2O_3 on the surface of the nanotubes.

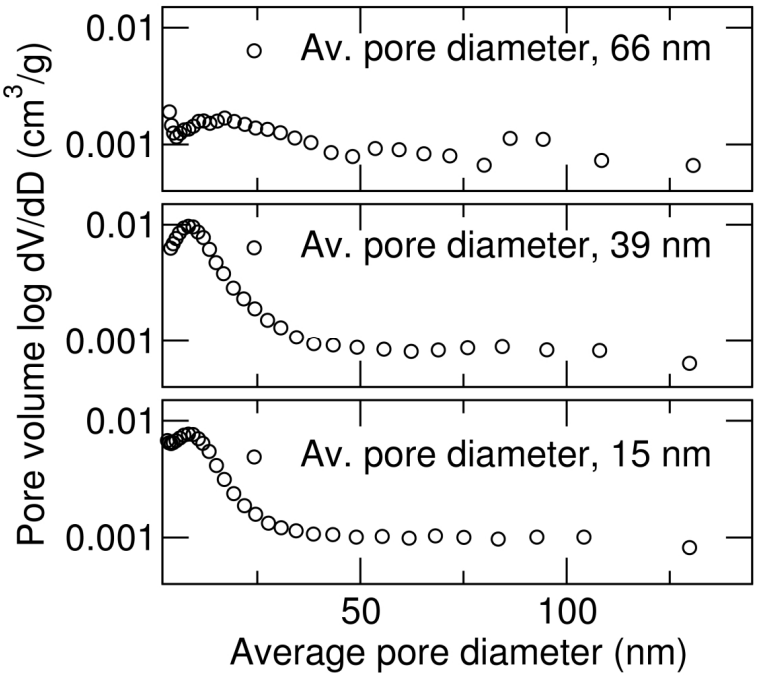

Figure 5. Barrett-Joyner-Halenda (BJH) pore size distributions from N_2 sorption isotherms of samples reduced for 6 h (from top to bottom: sample C, 400°C; sample F, 500°C ; sample J, 600°C). Note a reduction in the average pore size on increasing reduction times.

Thermogravimetric analysis of the resulting products indicates that the amine molecules act as sacrificial pore formers. An overall mass decrease of 35.4% was noted in the case of the original $V_2O_{5-\delta}$ nanoscrolls, due to the loss of the amine intercalant. We believe that the amine is burned out of the scrolls as reduction temperatures are increased. This reduces the total amount of amine present in the reduced products, which should be reflected in percentage weight losses in TGA. TGA curves plotted for samples reduced for 1 hour at 400°C and 600°C are shown in figure 6. The total mass loss for sample A (400°C, 1 h) is 9%, while for sample G (600°C, 1 h) this is reduced to 4.9%. This decrease in the amount of amine in the samples reduced at higher temperatures is due to the fact that there are a greater number of pores formed in these samples. Correspondingly, one would expect an increase in the surface areas with decreasing pore size. This is indeed the case, with a specific surface area of 33 m^2/g found for sample A (400°C, 1 h) and 66 m^2/g for sample G (600°C, 1 h).

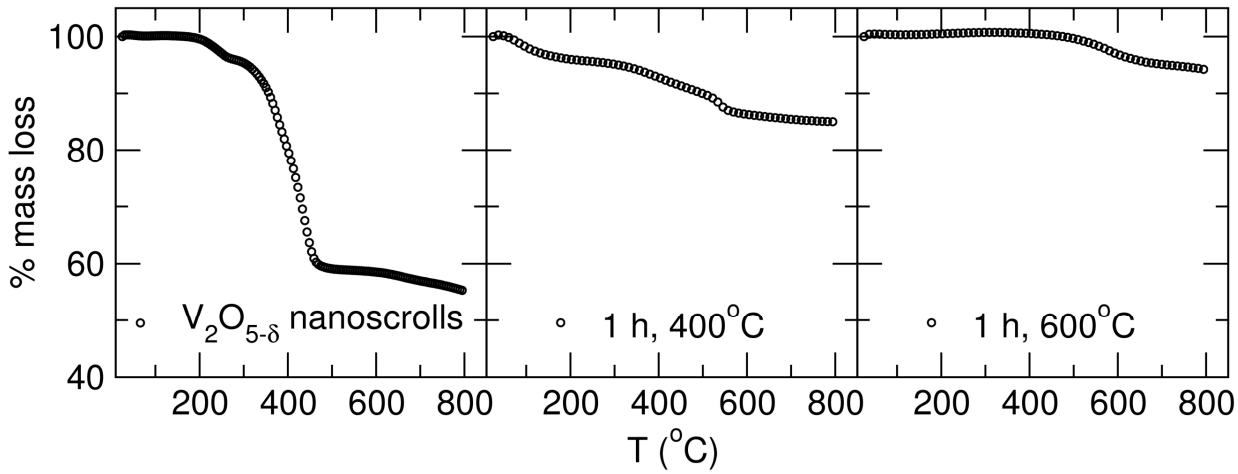

Figure 6. Thermogravimetric analysis of original nanoscrolls (left), rutile VO_2 sample A (middle) and corundum V_2O_3 sample G (right). Note the smaller mass loss for reductions carried out at higher temperatures due to the presence of less amine surfactant.

CONCLUSIONS

Reduction of a single phase nickel-manganese oxide precursor leads to the formation of porous, antiferromagnetic MnO, with ferromagnetic nickel nanoparticles formed from the leached nickel component. These nanoparticles are found to decorate the surface of the MnO matrix, with the majority of particles embedded within the matrix. SEM images show that the surface of the MnO is also covered with triangular facets and pores.

Rutile VO_2 and corundum V_2O_3 nanostructures may be formed by the controlled reduction of amine-templated $V_2O_{5-\delta}$ nanoscrolls. The porosity of these materials has been investigated by N_2 sorption measurements, with a decrease in pore size noted with increasing temperature. However, increased reduction times at high temperatures (600°C, 6 h) leads to the formation of nanocrystals on the nanotube surface, which causes a decrease in the observed specific surface area. TGA confirms the removal of the amine template during the reduction process leads to the formation of the porous structure.

ACKNOWLEDGMENTS

This work was supported by funding from the UC Discovery program and the American Chemical Society Petroleum Research Fund. We acknowledge the use of NSF-MRSEC (through No. DMR 0520415) and MRL facilities.

REFERENCES

1. Shchukin D G, Schattka J H, Antonietti M, Caruso R A, Photocatalytic properties of porous metal oxide networks by nanoparticle infiltration in a polymer gel template, *J. Phys. Chem. B* **107** 952-957 (2003)
2. Tiemann M, Porous metal oxides as gas sensors, *Chem. Eur. J.* **13** 8376-8388 (2007)

3. Owens B B, Passerini S, Smyrl W H, Lithium ion insertion in porous metal oxides, *Electrochimica Acta* **45** 215-224 (1999)
4. Toberer E S, Seshadri R, Spontaneous formation of macroporous monoliths of mesoporous manganese oxide crystals, *Adv. Mater.* **17** 2244-2246 (2005)
5. Toberer E S, Löfvander J P, Seshadri R, Topochemical formation of mesoporous MnO crystals, *Chem. Mater.* **18** 1047-1052 (2006)
6. Toberer E S, Epping J D, Chmelka B F, Seshadri R, Hierarchically porous rutile titania: harnessing spontaneous compositional change in mixed-metal oxides, *Chem. Mater.* **18** 6345-6351 (2006)
7. Toberer E S, Schladt T D, Seshadri R, Macroporous manganese oxides with regenerative mesopores, *J. Am. Chem. Soc.* **128** 1462-1463 (2006)
8. Nogués J, Sort J, Langlais V, Skumryev V, Suriñach S, Muñoz J S and Baró M D, Exchange bias in nanostructures, *Phys. Rep*. **422** 65–117 (2005)
9. Wickham D G, Solid-phase equilibria in the system NiO–Mn_2O_3–O, *J. Inorg. Nucl. Chem.* **26** 1369–77 (1964)
10. Corr S A, Grossman M, Furman J D, Melot B C, Cheetham A K, Keier K R, Seshadri R, Controlled reduction of vanadium oxide nanoscrolls: crystal structure, morphology and electrical properties, *Chem. Mater.* **20** 6396-6404 (2008)
11. Shoemaker D P, Grossman M and Seshadri R, Exchange biasing of single-domain Ni nanoparticles spontaneously grown in an antiferromagnetic MnO matrix, *J. Phys. Cond. Mat.* **20** 195219 (2008)